Geophysical Research Letters

RESEARCH LETTER
10.1029/2018GL080728

Key Points:
- We combine the largest-to-date set of 3-D dynamical models with observations to constrain the thermal state and interior structure of Mars
- Best-fit models suggest a core radius strictly larger than 1,800 km and an average crustal thickness 48.8 km $< d_c <$ 87.1 km
- Models suggest a large pressure dependence of the viscosity and a crust containing 65-70% of the total amount of heat producing elements

Supporting Information:
- Supporting Information S1
- Data Set S1
- Data Set S2

Correspondence to:
A.-C. Plesa,
Ana.Plesa@dlr.de

Citation:
Plesa, A.-C., Padovan, S., Tosi, N., Breuer, D., Grott, M., Wieczorek, M. A., et al. (2018). The thermal state and interior structure of Mars. *Geophysical Research Letters*, *45*, 12,198–12,209. https://doi.org/10.1029/2018GL080728

Received 22 AUG 2018
Accepted 5 NOV 2018
Accepted article online 9 NOV 2018
Published online 28 NOV 2018

©2018. American Geophysical Union. All Rights Reserved.

The Thermal State and Interior Structure of Mars

A.-C. Plesa[1], S. Padovan[1], N. Tosi[1,2], D. Breuer[1], M. Grott[1], M. A. Wieczorek[3], T. Spohn[1], S. E. Smrekar[4], and W. B. Banerdt[4]

[1]German Aerospace Center (DLR), Berlin, Germany, [2]Technische Universität Berlin, Berlin, Germany, [3]Université Côte d'Azur, Observatoire de la Côte d'Azur, CNRS, Laboratoire Lagrange, France, [4]Jet Propulsion Laboratory, California Institute of Technology, Pasadena, CA, USA

Abstract The present-day thermal state, interior structure, composition, and rheology of Mars can be constrained by comparing the results of thermal history calculations with geophysical, petrological, and geological observations. Using the largest-to-date set of 3-D thermal evolution models, we find that a limited set of models can satisfy all available constraints simultaneously. These models require a core radius strictly larger than 1,800 km, a crust with an average thickness between 48.8 and 87.1 km containing more than half of the planet's bulk abundance of heat producing elements, and a dry mantle rheology. A strong pressure dependence of the viscosity leads to the formation of prominent mantle plumes producing melt underneath Tharsis up to the present time. Heat flow and core size estimates derived from the InSight (Interior Exploration using Seismic Investigations, Geodesy and Heat Transport) mission will increase the set of constraining data and help to confine the range of admissible models.

Plain Language Summary We constrain the thermal state and interior structure of Mars by combining a large number of observations with thermal evolution models. Models that match the available observations require a core radius larger that half the planetary radius and a crust thicker than 48.8 km but thinner than 87.1 km on average. All best-fit models suggest that more than half of the planet's bulk abundance of heat producing elements is located in the crust. Mantle plumes may still be active today in the interior of Mars and produce partial melt underneath the Tharsis volcanic province. Our results have important implications for the thermal evolution of Mars. Future data from the InSight (Interior Exploration using Seismic Investigations, Geodesy and Heat Transport) mission can be used to validate our models and further improve our understanding of the thermal evolution of Mars.

1. Introduction

Tectonic and volcanic features on rocky planets like Mars are directly linked to processes in the interior that have been active for up to billions of years. A large volume of geophysical and geochemical data on the planet have become available from space missions and analyses of martian meteorites. Still, the thermal evolution of the interior is poorly known, and a number of issues are unsolved: (1) The large elastic lithosphere thickness underneath the north pole of Mars (Phillipsetal, 2008) is hard to reconcile with the well-accepted compositional model WD94 (Wänke & Dreibus, 1994), should this large elastic thickness be representative of the global average. The WD94 model is based on element correlations measured for the martian meteorites and shows Th/K ratios in close agreement with the surface abundance of heat producing elements, HPE (Taylor et al., 2006). Since the WD94 heat production rate implies a smaller average elastic lithosphere thickness than the north pole estimate, it has been argued that the bulk abundance of HPE in Mars could be lower than previously estimated by geochemical models (Phillips et al., 2008) or that the north pole elastic thickness is not representative of the entire planet (Grott & Breuer, 2010; Kiefer & Li, 2009; Phillips et al., 2008; Plesa et al., 2016). (2) The surface abundance of HPE derived from gamma-ray measurements indicate a significant enrichment of HPE in the crust, suggesting a present-day crustal heat production rate of 49 pW/kg (Hahn et al., 2011; Taylor et al., 2006). However, gamma-ray measurements can only map the uppermost 10 cm of the crust, and little is known about the HPE distribution in deeper layers. (3) Gravity and topography data have been used to derive maps of the thickness of the martian crust. The results are non-unique; inferred crustal thicknesses vary between 30 and 87 km for uniform crustal densities between 2,700 and 3,200 kg/m^3 (Plesa et al., 2016; Wieczorek & Zuber, 2004). In addition, the difference in crustal thickness between the northern and southern

hemispheres (the so-called crustal thickness dichotomy) can be reduced if the crustal density varied between the two hemispheres (Goossens et al., 2017; Plesa et al., 2016). (4) Large volcanic provinces such as Tharsis and Elysium have been active over most of the evolution of Mars (e.g., Hauber et al., 2011; Neukum et al., 2004; Werner, 2009) suggesting the presence of long-lived mantle plumes. Whether such mantle plumes are still active today is unknown. (5) Planet formation scenarios as well as geological and petrological evidence suggest that the martian mantle must have contained at least few tens of parts per million (ppm) water (e.g., Brasser, 2013; Dreibus & Wänke, 1985) at the end of accretion, sufficient for significant rheological weakening (Hirth & Kohlstedt, 2003; Karato & Wu, 1993). The initial mantle inventory was likely reduced by dehydration during partial melting (e.g., Morschhauser et al., 2011), but the present-day water concentration in the mantle and its rheological significance is much-debated (see Filiberto, Baratoux, et al., 2016, for a recent review). Constraints on the present-day water inventory in the interior of Mars come from the analysis of martian meteorites. Recent studies suggest a water content < 130 ppm (Filiberto, Gross, et al., 2016) and even as low as $14 - 23$ ppm from the analysis of depleted shergottites (McCubbin et al., 2016).

Parameterized as well as 2-D and 3-D convection models (Breuer & Moore, 2015) of the thermal evolution of Mars have been used to explain, for example, the formation of the crustal thickness dichotomy, the formation of a super plume underneath Tharsis (e.g., Golabek et al., 2011; Keller & Tackley, 2009; Roberts & Zhong, 2006), and the magmatic and crust formation history (e.g., Breuer & Spohn, 2006; Fraeman & Korenaga, 2010; Hauck & Phillips, 2002; Morschhauser et al., 2011; Plesa & Breuer, 2014; Ruedas et al., 2013). Other mantle convection models studied the cooling and solidification of a putative liquid magma ocean (e.g., Elkins-Tanton et al., 2005; Maurice et al., 2017; Plesa et al., 2014; Tosi, Plesa, et al., 2013) and the effects of large-scale impacts on the interior dynamics (e.g., Roberts & Arkani-Hamed, 2017; Ruedas & Breuer, 2017). In this study we compare the results of the largest set of numerical simulations to date of the thermal evolution of Mars in 3-D spherical geometry with available observations in order to identify key parameters that control the interior evolution. The calculations will provide a tool to support the overall interpretation of data from the upcoming Interior exploration using Seismic Investigations, Geodesy and Heat Transport (InSight) mission (Banerdt & Russell, 2017), which will deploy a seismometer and a heat flow probe in the Elysium Planitia region on Mars to record seismic data and measure the surface heat flow for a martian year.

2. Methods

We ran 130 models in 3-D spherical geometry using the mantle convection code Gaia (Hüttig & Stemmer, 2008a, 2008b; Hüttig et al., 2013). Model details are described in Plesa et al. (2015, 2016) and in supporting information S1. In our models we varied the following input parameters: initial mantle temperature, core size, mantle reference viscosity, pressure, and temperature dependence of the viscosity (Hirth & Kohlstedt, 2003; Karato & Wu, 1993), a constant or a temperature- and pressure-dependent mantle thermal expansivity (Tosi, Yuen, et al., 2013), thickness and thermal conductivity of the crust, and the amount and distribution of HPE in the interior. Most simulations employ the bulk abundance of HPE of the WD94 compositional model, but some cases assume a lower amount (see Table S1). All simulations consider a nominally anhydrous mantle. However, we test reference viscosities between 10^{20} Pa s, considering the viscosity lowering due to the presence of a few tens of ppm water (Hirth & Kohlstedt, 2003; Karato & Wu, 1993), and 10^{21} Pa s, corresponding to a dry mantle rheology. We use crustal thickness models derived from gravity and topography data that we keep constant in time. Crustal densities vary between 2,700 and 3,200 kg/m^3, and for one model, we employ a density of 2,900 kg/m^3 for the southern highlands and 3,100 kg/m^3 for the northern lowlands using the dichotomy boundary of Andrews-Hanna et al. (2008). Further details of the crustal thickness models are discussed in Wieczorek et al. (2013) and Plesa et al. (2016). The crust is homogeneously enriched in HPE, such that we obtain a present-day heat production rate $H_{cr} = 49$ pW/kg in agreement with gamma-ray data (see supporting information S1 for further details). As the concentration of HPE in the deep crust is poorly known, we tested the sensitivity of our results by running additional cases, for which the present-day H_{cr} lies between 9.8 and 98 pW/kg (i.e., 5 times lower and 2 times higher than the average value suggested by gamma-ray data).

All constraints considered are related to the interior temperature distribution, either directly (potential temperature inferred from shergottite mineralogy and occurrence of present-day melting) or indirectly (tidal Love number k_2, dissipation factor Q, and elastic lithosphere thickness). The tidal Love number k_2 provides a strong constraint on the interior structure of the planet, given its sensitivity to the size of the liquid core (Rivoldini et al., 2011; Van Hoolst et al., 2003; Yoder et al., 2003). A detailed description of the constraints used is given in supporting information S1.

19448007, 2018, 22, Downloaded from https://agupubs.onlinelibrary.wiley.com/doi/10.1029/2018GL080728 by Cochrane Colombia, Wiley Online Library on [24/06/2025]. See the Terms and Conditions (https://onlinelibrary.wiley.com/terms-and-conditions) on Wiley Online Library for rules of use; OA articles are governed by the applicable Creative Commons License

We compute k_2 at the period of the semidiurnal Solar tide for the entire set of convection models (Moore & Schubert, 2000; Padovan et al., 2014) and find only the subset of models with a radius of 1,850 km to be compatible with the most recent estimate for this observable, $k_2 = 0.169 \pm 0.006$ (Konopliv et al., 2016). In computing k_2, we use the Andrade pseudoperiod model (Jackson et al., 2010; Padovan et al., 2014), which accounts for the nonelastic response of mantle rock at tidal frequencies, to obtain a rheological profile (see model description in supporting information S1). Thus, as part of the calculation, we estimate the tidal quality factor Q at the semidiurnal tide of Phobos. Our result is in line with previous work: Yoder et al. (2003) provide a range of core radii between 1,520 and 1,840 km for k_2 ranging between 0.136 and 0.170; Rivoldini et al. (2011) find the core radius between 1,800 and 1,900 km for a k_2 of 0.17. A recent study (Khan et al., 2017) that applied an inversion technique similar to the one used in Rivoldini et al. (2011), obtained slightly smaller core radii between 1,730 and 1,840 km when using the latest k_2 estimate (Genova et al., 2016; Konopliv et al., 2016). The small discrepancy between their and our result is likely due to differences in the viscoelastic model employed (Khan et al., 2017).

Q is mostly sensitive to the viscosity profile (Nimmo & Faul, 2013), which in turn depends strongly on the mantle temperature, the grain size, and possibly the iron content (Zhao et al., 2009). While a number of parameters enter the calculation of Q and some of them are not well known for Mars (see additional discussion in supporting information S1), for a given core radius the hotter the mantle, the lower is Q (i.e., the more dissipative is the mantle). By computing Q for each convection model—allowing for variations of unknown parameters (e.g., activation energy)—and comparing the results with the range 99.5 ± 4.9 inferred from the orbital acceleration of Phobos (Konopliv et al., 2011; Lainey, 2016), we find that models with inefficient heat transport remain too hot (i.e., too dissipative) to satisfy the tidal quality factor constraint. This may be caused by a too large pressure dependence of the viscosity (e.g., an activation volume of 20 cm^3/mol) or by a too large concentration of HPE in the mantle. The latter may be caused by either a low crustal enrichment (e.g., present-day H_{cr} of only 9.8 pW/kg) or, alternatively, by a crust thinner than 45 km with present-day $H_{cr} = 49$ pW/kg as suggested by the gamma-ray data. Conversely, the mantle is too cold and not dissipative enough if the HPE concentration in the mantle is too small. The latter is observed for models with $H_{cr} = 49$ pW/kg at present day and an average crustal thickness ≥ 87 km.

By calculating the mechanical lithosphere thickness, we obtain an upper bound for the elastic lithosphere thickness (see supporting information S1 for mechanical lithosphere thickness calculations), which we compare with available estimates for the Noachian epoch and for the present-day north and south polar regions. The mechanical lithosphere thickness can be mapped by tracing the isotherm that is associated with the onset of ductile deformation (Burov & Diament, 1995). That thickness is similar to the effective elastic thickness if the lithospheric plate has a small curvature and bending moment (McNutt, 1984). A small elastic lithosphere thickness for the Noachian suggests a thin thermal boundary layer, vigorous mantle convection, and/or a warm lithosphere (Grott et al., 2013). A warm lithosphere can be obtained if the bulk of the crust has already been emplaced during the Noachian and contains >40% of the total HPE inventory of the WD94 compositional model. Present-day localized melting, the high potential temperatures inferred from the mineralogy of the shergottites (Filiberto & Dasgupta, 2015), and a present-day elastic lithosphere thickness of at least 110 km at the south pole of Mars (Wieczorek, 2008) require a mantle moderately depleted in HPE and a crust thinner than 87 km on average. Models with an average crustal thickness of 87 km and present-day $H_{cr} = 49$ pW/kg have a strongly depleted mantle that cools too rapidly and does not produce melt late in the thermal evolution, not even locally. At the same time, the elastic thickness values are smaller than the available present-day south pole estimate, due to the insulating effect of the thick southern crust. Decreasing the crustal heat production rate would lead to smaller lithospheric temperatures and consequently to a thicker present-day elastic lithosphere at the south pole but would suggest an elastic lithosphere in the Noachian thicker than estimated.

3. Results

The results of our 130 thermal evolution calculations are summarized in Figure 1, and the nine best-fit models (cases 51, 84, 85, 94, 97, 117, 118, 121, and 129 in Table S2) are identified. All best-fit models share a dry mantle rheology with a reference viscosity of 10^{21} Pa s and a wet crustal rheology. The latter is required to obtain small elastic lithosphere thickness values for the Noachian epoch. Some successful models have a large activation volume of 10 cm^3/mol implying a strong pressure dependence of the viscosity. Others (cases 117 and 118) have a moderate value of 6 cm^3/mol but adopt a proposed 50-fold viscosity increase in the mid-mantle, possibly caused by a mineralogical transition zone (Keller & Tackley, 2009). All successful models are

19448007, 2018, 22, Downloaded from https://agupubs.onlinelibrary.wiley.com/doi/10.1029/2018GL080728 by Cochrane Colombia, Wiley Online Library on [24/06/2025]. See the Terms and Conditions (https://onlinelibrary.wiley.com/terms-and-conditions) on Wiley Online Library for rules of use; OA articles are governed by the applicable Creative Commons License

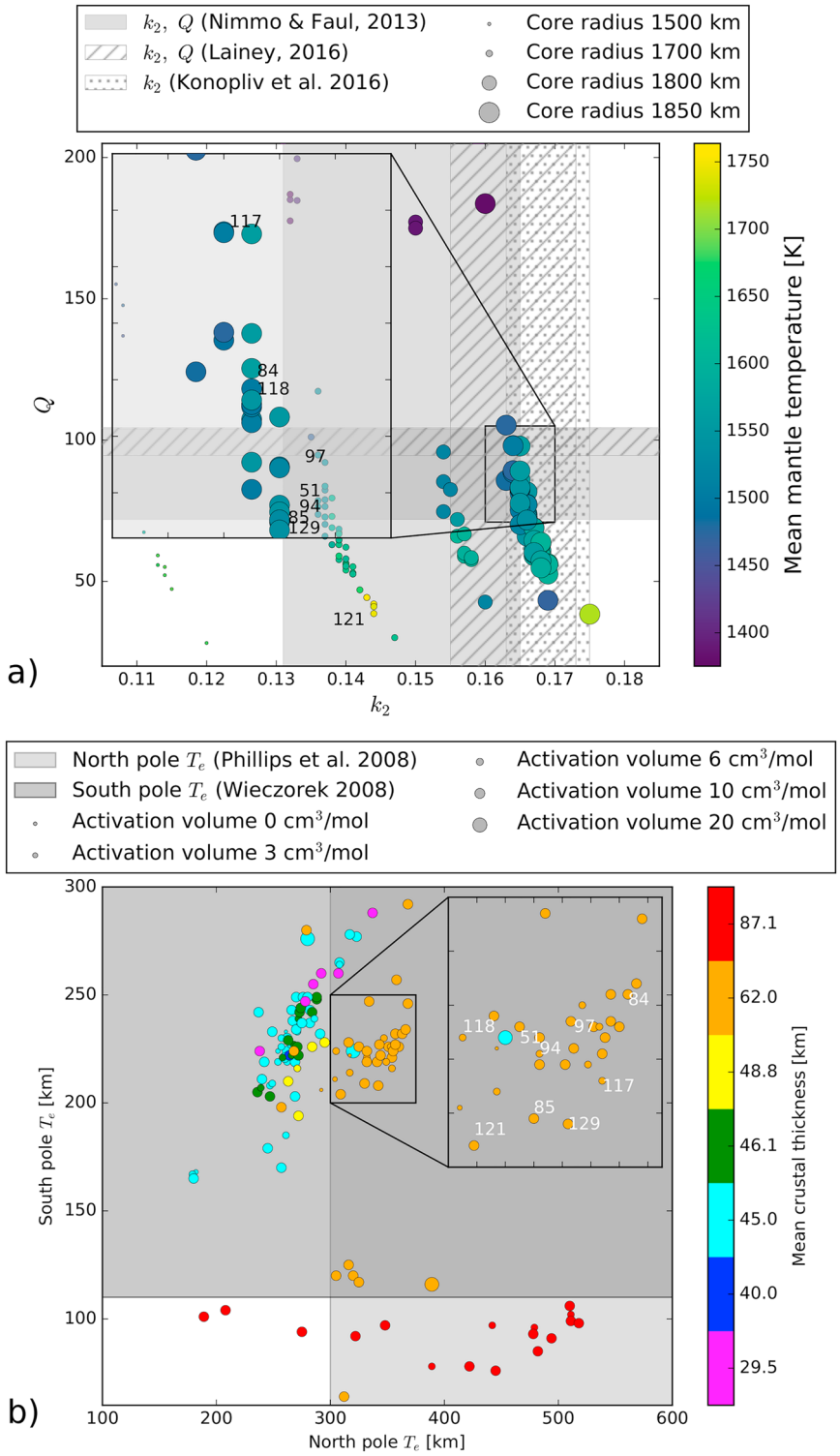

Figure 1. Results of the model calculations comparing tidal parameter and present-day elastic lithosphere thickness constraints. (a) k_2 and Q. Each symbol represents one model. The size of the symbols is proportional to the size of the core as given in the legend. Colors indicate the mean mantle temperature. (b) Present-day elastic lithosphere thickness values underneath the polar caps which extend to 5° from the south and 10° from the north pole. The size of the symbols shows the activation volume and hence indicates the strength of the pressure dependence of the viscosity. Colors show the average crustal thickness used in the simulations. Best-fit models are indicated by their case number (See Table S1 for the parameters of these models). The gray and hatched areas on both panels show available estimates for k_2, Q, and the elastic lithosphere thicknesses at the north and south poles of Mars. Note that the areas of successful models have been enlarged for clarity in both panels.

19448007, 2018, 22, Downloaded from https://agupubs.onlinelibrary.wiley.com/doi/10.1029/2018GL080728 by Cochrane Colombia, Wiley Online Library on [24/06/2025]. See the Terms and Conditions (https://onlinelibrary.wiley.com/terms-and-conditions) on Wiley Online Library for rules of use; OA articles are governed by the applicable Creative Commons License

characterized by inefficient heat transport from the deep mantle caused by the large viscosity there. The viscosity of the lower mantle is 9 to 721 times higher than that of the upper mantle in these models. Average temperature profiles are similar for cases using a small and a large activation volumes (i.e., 0 and 10 cm^3/mol), but the temperature variations are larger by more than 160 K for the case using a large pressure dependence of the viscosity (Figure S4). As the mantle cools and the thermal lithosphere on top of the convecting mantle thickens, the viscosity contrast across the convecting mantle decreases in time (Figure S5).

The average crustal thickness of all best-fit models is 62 km, in agreement with the upper range of values found by Wieczorek and Zuber (2004), and the crust is strongly enriched in HPE, with a present-day H_{cr} of 44.1–49 pW/kg. Cases with a thinner crust require H_{cr} at least 1.2 and 1.7 times higher than the gamma-ray measurements for crustal thicknesses of 45 and 29.5 km, respectively, to satisfy the large present-day elastic lithosphere thickness at the north pole (cases 109 and 126). However, a large enrichment of the crust makes it difficult to obtain present-day melting in the mantle, even when using the most recent solidus estimates of the martian mantle (Kiefer et al., 2015; Ruedas & Breuer, 2017), as the latter is considerably depleted. In addition, a thin crust is less efficient in insulating the mantle. Crustal heat production rates higher than the ones suggested by the gamma-ray data cannot be excluded on a local scale. However, they are not likely to be globally representative as this would result in large-scale remelting of the basaltic crust. Since there is no evidence for widespread tertiary crust in the gamma-ray data (Taylor et al., 2006), we consider models employing a crustal enrichment in HPE larger than the value suggested by gamma-ray measurements only marginally relevant.

All best-fit models have a large core with a radius of 1,850 km for consistency with the latest k_2 estimate of 0.169 ± 0.006 (Konopliv et al., 2016). A core radius of 1,850 km also helps to explain the presently thick elastic lithosphere underneath the north pole as a thinner mantle contains smaller amounts of HPE when compared to models with a smaller core. However, the high potential temperatures required by the shergottite mineralogy are more difficult to explain for large core models. For a core radius of 1,500 km, high mantle temperatures are easily obtained, but the present-day elastic thicknesses at the north and south poles of Mars cannot be matched. If we consider smaller k_2 values of 0.136, this would allow models with a smaller core radius (models 41, 42, and 130 have core radii of 1,700 and 1,800 km). Other parameters of these models are similar to those of the nine best-fit models.

The present-day elastic lithosphere thicknesses at the north and south poles of Mars constitute a particularly tight constraint. If we relaxed the limit of $\geq$300 km for the north polar elastic lithosphere thickness by 20 km and that for the south pole of $\geq$110 km by 10 km, three additional models would satisfy the requirements (cases 88, 110, and 120 in Table S1). While the rheological parameters remain unchanged from the nine best-fit cases, models with an average crustal thickness of 45 km (cases 110 and 120) and 46 km (case 88) become acceptable. In addition, if both the present-day elastic thicknesses and the k_2 estimate are relaxed, another case employing a crustal thickness of 48.8 km becomes compatible with observations (case 36). Still, the crustal HPE content needs to be high, requiring a present-day H_{cr} to be 49–59 pW/kg.

The most relevant parameters of the best-fit models are listed in Table 1, while lists of all parameters and results for each individual model are included in supporting information S1.

In the following, we discuss a model representative of the nine best-fit models in more detail (Figure 2). Although we will be referring to this model as the *reference model*, we emphasize that it is by no means better than the other eight models. The reference model (case 85) differs from other best-fit models by having a high initial mantle temperature of 1,850 K compared to 1,650 K used in cases 84, 117, and 129, a slightly higher activation energy of 325 kJ/mol compared to 300 kJ/mol used in case 51. Cases 117 and 118 employ a smaller activation volume of only 6 cm^3/mol but use an additional 50-fold viscosity increase in the midmantle. In the reference case we use the WD94 compositional model, but other best-fit models use a smaller amount of HPE than WD94 by assuming a lower concentration by up to 10% in the crust (case 94) or in the mantle (case 97). The effects of varying the HPE abundances are discussed in supporting information S1.

We note that all nine best-fit models show present-day mantle plumes underneath Tharsis and Elysium, with the Tharsis plume still producing partial melt today. The location of mantle plumes is affected by the crustal thickness distribution and crustal content of HPE. Mantle plumes either originate or migrate during the first billion year of evolution beneath regions covered by a thick insulating crust. This has been observed also in previous studies that have investigated the thermal insulation of a thick crust (Schumacher & Breuer, 2006)

19448007, 2018, 22, Downloaded from https://agupubs.onlinelibrary.wiley.com/doi/10.1029/2018GL080728 by Cochrane Colombia, Wiley Online Library on [24/06/2025]. See the Terms and Conditions (https://onlinelibrary.wiley.com/terms-and-conditions) on Wiley Online Library for rules of use; OA articles are governed by the applicable Creative Commons License

Table 1
Mantle Parameters of the Best-Fit Models

Parameter	Value	Unit
Core radius[a]	>1,800	km
Average crustal thickness[b]	$48.8 < d_c < 87.1$	km
Initial bulk abundance of HPE	21.3–23	pW/kg
Present-day bulk abundance of HPE	3.8–4.1	pW/kg
Initial crustal heat production rate	247.5–275	pW/kg
Present-day crustal heat production rate	44.1–49	pW/kg
Mantle reference viscosity	10^{21}	Pa s
Activation volume	10 or 6 with additional 50-fold viscosity increase	cm^3/mol
Present-day mantle HPE (of the present-day bulk HPE inventory)[c]	30–34.6%	—

Note. The values are compatible with all observational constraints used in this study. See supporting information S1 for additional parameters used in each individual thermal evolution model. HPE = heat producing elements.
[a]All best-fit models use a core radius of 1,850 km. While slightly smaller or larger core radii may fit the k_2 estimate, no model with a core radius of 1,800 km has been found admissible. [b]All best-fit models use an average crustal thickness of 62 km. Although a slightly thinner or thicker crust might fit the observations, no models using an average crustal thickness of 48.8 km or thinner and no cases using an average crustal thickness of 87.1 km have been found compatible with our constraints. [c]Computed as $100 \cdot (H_m \cdot M_m)/(H_{bulk} \cdot M_{silicate})$, where H_m and H_{bulk} are the heat production rate in the mantle and the bulk inventory of HPE, respectively, while M_m and $M_{silicate}$ are the mass of the mantle and the total silicate mass, respectively.

or modeled the migration of the Tharsis plume caused by differential rotation of the lithosphere (Šrámek & Zhong, 2012; Zhong, 2009). Plume migration could have been also caused by a large-scale impact onto the northern hemisphere, whose ejecta distribution led to a thick insulating southern hemisphere (Citron et al., 2018). Furthermore, a Tharsis plume track has been inferred from geologic units and crustal magnetic anomalies in the southern hemisphere (Hynek et al., 2011) and has been found consistent with a path of thick crust, which was identified in crustal thickness models accounting for rotational effects on shape and geoid (Cheung & King, 2014).

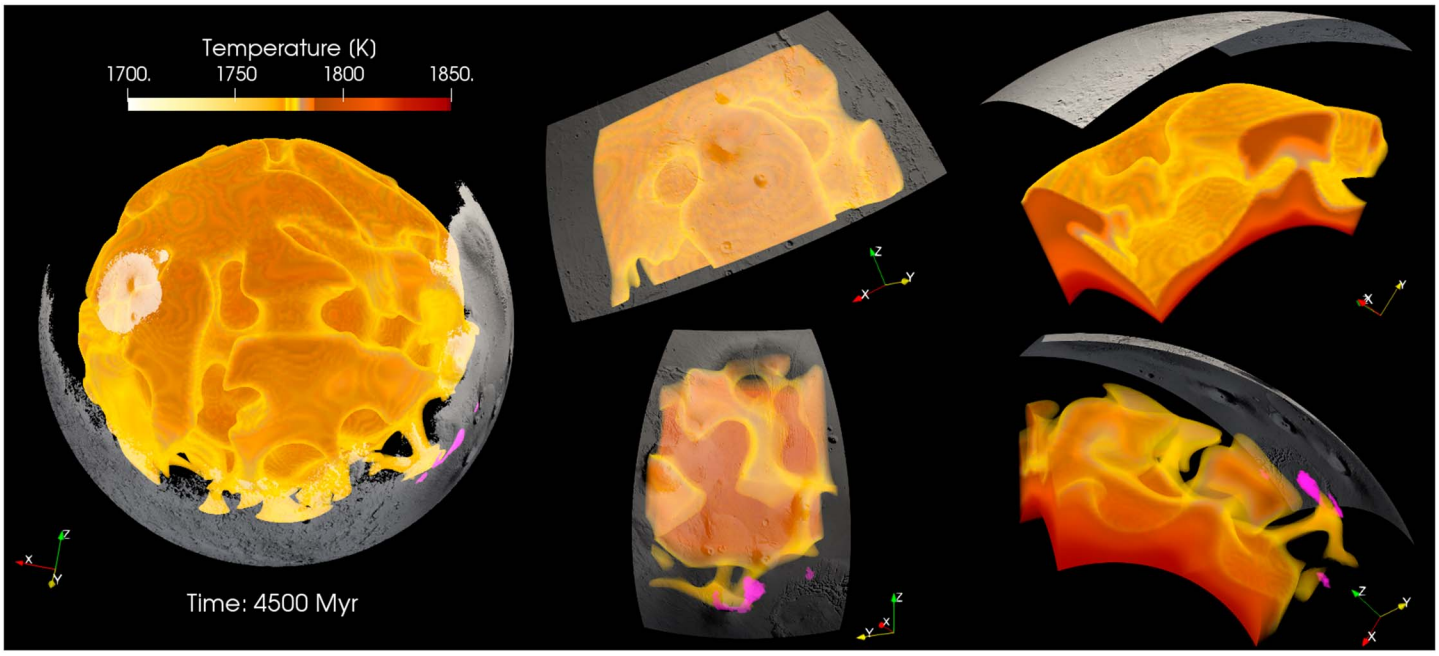

Figure 2. Present-day convection pattern. Mantle plumes of the reference model (case 85 in supporting information S1) are located underneath the large volcanic centers Tharsis (top row right) and Elysium (bottom row right). Although there are mantle plumes in addition to the ones underneath Tharsis and Elysium, we note that the Tharsis plume is stable through most of the thermal evolution and produces partial melt up to the present day (shown in pink color). The surface of Mars is based on a Mars Orbiter Laser Altimeter shaded relief map, which was converted to gray scale colors and shows only regions covered by a thick crust.

19448007, 2018, 22, Downloaded from https://agupubs.onlinelibrary.wiley.com/doi/10.1029/2018GL080728 by Cochrane Colombia, Wiley Online Library on [24/06/2025]. See the Terms and Conditions (https://onlinelibrary.wiley.com/terms-and-conditions) on Wiley Online Library for rules of use; OA articles are governed by the applicable Creative Commons License

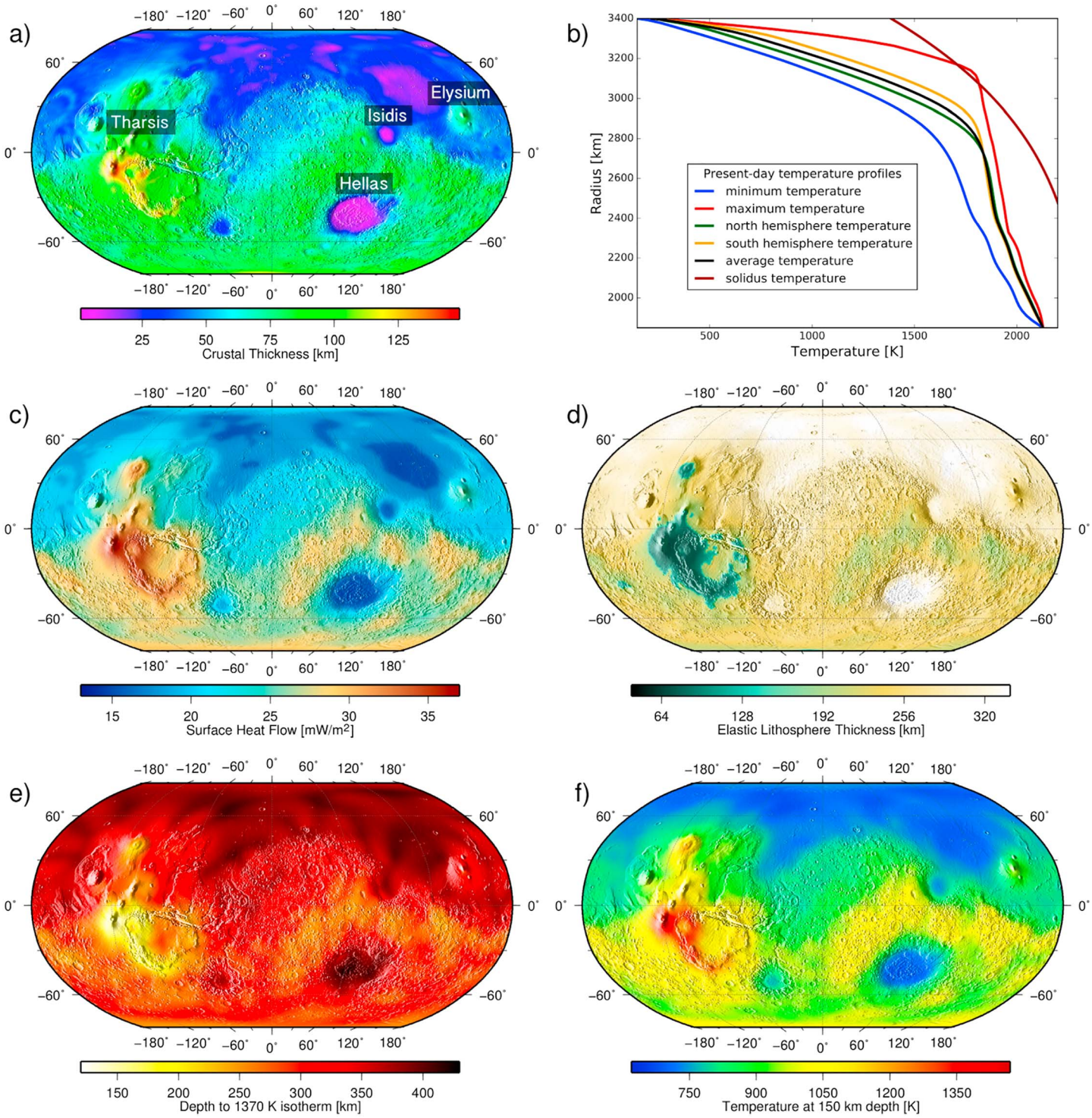

Figure 3. Crustal thickness distribution (a) and temperature profiles through the mantle (b) as well as maps of the surface heat flow (c), elastic lithosphere thickness (d), depth to the 1,370-K isotherm (e), and temperature at 150-km depth (f) for the reference model at present day. The model assumes a lower thermal conductivity of the crust compared to the mantle (3 vs. 4 $W \cdot m^{-1} \cdot K^{-1}$). The elastic thickness has been computed using the deformation time scale given by the polar cap deposition to have a better comparison with the present-day elastic thickness at the north pole. The temperature profile underneath the northern hemisphere has been computed for regions covered by a crust smaller than the average crustal thickness while for the southern hemisphere for regions covered by a crust larger than or equal to the average value.

19448007, 2018, 22, Downloaded from https://agupubs.onlinelibrary.wiley.com/doi/10.1029/2018GL080728 by Cochrane Colombia, Wiley Online Library on [24/06/2025]. See the Terms and Conditions (https://onlinelibrary.wiley.com/terms-and-conditions) on Wiley Online Library for rules of use; OA articles are governed by the applicable Creative Commons License

The long-wavelength topographic and geoid anomalies at degree 2 and 3 associated with the Tharsis province are best explained by volcanic loading and downward displacement of the lithosphere rather than in terms of dynamic uplift by a mantle plume (Zhong & Roberts, 2003), an inference that is also consistent with the observed fault patterns around the region (Banerdt et al., 1992). The plume beneath Tharsis in our reference model agrees with this scenario. Although it generates a substantial dynamic geoid, it contributes to the power spectrum only at degrees between about 4 and 8.

Figures 3a and 3b show the crustal thickness model, which was employed in this specific case, and temperature profiles throughout the mantle at present day, respectively. The largest temperature differences are found in the uppermost 500 km and are caused by the combined effect of crustal thickness variations, HPE content of the crust, and the underlying convection pattern. We observe a clear dichotomy in temperature for the uppermost 600 km (green and orange lines in Figure 3b), reflecting the difference between the thick insulating crust in the southern hemisphere and the thin crust in the northern hemisphere, which allows for a stronger cooling of the underlying northern hemisphere mantle. In fact, such a temperature distribution pattern is found for all best fit-models, with peak-to-peak variations of 753–891 K at depths of 211–260 km. The large temperature variations predicted from our models may imply a seismic wave velocity dichotomy in the mantle and should be considered for the interpretation of InSight seismic data.

The variations of the present-day surface heat flow, elastic lithosphere thickness, of the depth to the 1,370-K isotherm marking the bottom of the stagnant-lid, and of temperature distribution at 150-km depth (Figures 3c–3f, respectively) closely mirror the crustal thickness variations showing a small heat flow and large elastic thickness in regions overlain by a thin crust (e.g., Hellas and Isidis impact basins). Large heat flow and small elastic thickness values are observed for the Tharsis province where the crust is thick. Some local areas, in particular in the southern hemisphere around Hellas and in and around the Tharsis region, show the presence of mantle plumes through a relatively high heat flow (Figure 3c), a thin elastic thickness (Figure 3d), shallow depth to the 1,370-K isotherm (Figure 3e), and a relatively high temperature compared to surrounding regions (Figure 3f). These mantle plumes might have once fed volcanoes like Tyrrhena and Malea Patera of the Circum-Hellas volcanic province or Nili and Meroe Patera of the Syrtis Major province.

4. Discussion

Earlier studies using parameterized convection models required a rheologically significant amount of water in the martian mantle to explain the thin elastic lithosphere inferred for the Noachian (Grott & Breuer, 2008, 2009). These studies assumed a uniform crustal thickness, while ours includes a suite of spatially varying crustal thickness models based on geophysical data. We find the interior of Mars to have a high reference viscosity representative of a dry mantle rheology, in agreement with other recent petrological and geodynamical studies (Breuer et al., 2016; Filiberto, Gross, et al., 2016; McCubbin et al., 2016; Thiriet et al., 2018). The thick crust covering the southern hemisphere together with a significant enrichment in HPE as suggested by gamma-ray spectroscopy data allows a thin elastic lithosphere during the Noachian even for a dry mantle. In fact, if the interior of the planet had contained significant amounts of water, our results require that much of the water must have been lost to the atmosphere and/or stored in the crust early on, for example, through crust formation. A wet mantle rheology during most of the evolution would have resulted in significant cooling of the interior and weaker present-day mantle plumes, which cannot be reconciled with evidence for recent local high mantle temperatures (Filiberto, 2017; Filiberto & Dasgupta, 2015; Kiefer & Li, 2016; Musselwhite et al., 2006). This conclusion strengthens similar conclusions from previous 1-D models (Morschhauser et al., 2011).

Our results suggest that the martian mantle viscosity strongly increases with pressure and indicate an activation volume $V = 10\,\mathrm{cm}^3/\mathrm{mol}$. This value is higher than values used in previous geodynamical models (e.g., Keller & Tackley, 2009; Kiefer & Li, 2016; Plesa & Breuer, 2014; Ruedas et al., 2013; Šrámek & Zhong, 2012) but agrees with recent rheological studies for Mars and the upper mantle of the Earth (Dixon & Durham, 2018; Raterron et al., 2017). The large pressure dependence can explain the formation and stability of prominent mantle plumes implying spatial temperature variations in the deep mantle. At shallower depths ($\leq$600 km), however, temperature is mostly controlled by the crustal thickness pattern with mantle plumes imprinting smaller additional variations.

Our models require that the bulk of the crust was formed early in the history of Mars such that the thick insulating crust over the southern hemisphere leads to small elastic lithosphere thicknesses during the Noachian epoch. Indeed, geological evidence suggests that the bulk of the crust has been built early during

19448007, 2018, 22, Downloaded from https://agupubs.onlinelibrary.wiley.com/doi/10.1029/2018GL080728 by Cochrane Colombia, Wiley Online Library on [24/06/2025]. See the Terms and Conditions (https://onlinelibrary.wiley.com/terms-and-conditions) on Wiley Online Library for rules of use; OA articles are governed by the applicable Creative Commons License

the planetary evolution (Greeley & Schneid, 1991; Nimmo & Tanaka, 2005). All our best-fit models use a 62-km-thick crust with a uniform density of 3,100 kg/m^3, in excellent agreement with petrological analyses of martian meteorites and surface rocks (Baratoux et al., 2014). A present-day crustal heat production rate of 44.1–49 pW/kg is in good agreement with the gamma-ray measurements (Hahn et al., 2011) and with a recent study (Thiriet et al., 2018), which employed parameterized thermal evolution models to investigate the thickness and enrichment of the southern and northern martian crusts. The present-day mantle would then contain only about 30–35% of the current bulk HPE inventory. Models employing a crust of 45 km or thinner require a higher crustal heat production rate to match the present-day thick elastic lithosphere at the north pole and at the same time have difficulties to explain recent melt production in the interior.

The lower amount of Th and K obtained by the analyses of martian meteorites led to the conclusion that crustal HPE content might decrease with depth (Newsom et al., 2007). However, models with a mantle HPE content higher than 52% of the bulk WD94 compositional model cannot obtain a large present-day elastic thickness at the north pole of Mars. Although the analyses of martian meteorites and surface rocks at Gale crater seem to indicate larger differences in the crustal HPE content (Sautter et al., 2016), the gamma-ray data show little spatial variation in the surface abundance of HPE (Hahn et al., 2011). This suggests that the variations indicated by meteorites and surface rocks samples are on spatial scales below the resolution of our models and do not affect our conclusions.

The most recent k_2 estimates can be matched if the core radius is $\geq$1,850 km. While slightly smaller or larger core radii may fit the latest k_2 estimates, our models require that the core radius is strictly larger than 1,800 km. Thus, our models confirm previous studies of the interior structure of Mars (Rivoldini et al., 2011). A large core would contain a significant amount of light constituent to match mass and moment of inertia constraints. If sulfur were the only light element, about 17 wt% (Rivoldini et al., 2011) would be required. This much sulfur places the core close to the eutectic composition and suggests a melting temperature smaller than 1,600 K. Thus, the core would most likely be entirely liquid today as has been suggested by Schubert and Spohn (1990).

5. Conclusions

We have employed the largest-to-date set of numerical simulation of thermal evolution in a 3-D geometry and used a considerable number of observational data to constrain the thermal state and interior structure of Mars. Our models suggest a core radius strictly larger than 1,800 km and an average crustal thickness larger than 48.8 km but lower than 87.1 km, with an average crustal density between 3,000 and 3,200 kg/m^3. In addition, a large amount of HPE in the crust (i.e., 65.4–70 % of the bulk HPE inventory) and a large pressure dependence of the viscosity (i.e., an activation volume $V = 10$ cm^3/mol) are required to match the observations. A smaller core and a thinner crust or a crust more enriched in HPE could match the observations provided that the k_2 and the north and south pole present-day elastic thickness constraints are relaxed. However, the rheological parameters (i.e., a large pressure dependence of the viscosity and a dry mantle rheology) would not be affected, suggesting that the martian mantle viscosity is robustly constrained. Future data on the crustal thickness and core size as well as direct estimates of the surface heat flow from the InSight mission can be used to validate our findings and further improve our models.

Acknowledgments
We thank Walter S. Kiefer and an anonymous reviewer for their thoughtful comments, which helped to improve a previous version of this manuscript. All the parameters used in the models and their outcomes are listed in the online supporting information. S. P. acknowledges support by the DFG within the Research Unit FOR 2440 "Matter Under Planetary Interior Conditions". N. T. acknowledges support from the Helmholtz Gemeinschaft (project VH-NG-1017). S. E. Smrekar and W. B. Banerdt were supported by the InSight Project, Jet Propulsion Laboratory, California Institute of Technology, under a contract with the National Aeronautics and Space Administration. Computational time has been provided by the HLRN (project bep00064), which is gratefully acknowledged. This is InSight Publication No. 65.

References

Andrews-Hanna, J. C., Zuber, M. T., & Banerdt, W. B. (2008). The Borealis basin and the origin of the martian crustal dichotomy. *Nature*, *453*, 1212–1215. https://doi.org/10.1038/nature07011

Banerdt, W. B., Golombek, M. P., & Tanaka, K. L. (1992). Stress and tectonics on Mars. In M. George (Ed.), *Mars* (pp. 249–297). Pasadena, CA: JPL.

Banerdt, W. B., & Russell, C. T. (2017). Editorial on: Topical collection on InSight mission to Mars. *Space Science Reviews*, *211*(1), 1–3. https://doi.org/10.1007/s11214-017-0414-0

Baratoux, D., Samuel, H., Michaut, C., Toplis, M. J., Monnereau, M., Wieczorek, M., et al. (2014). Petrological constraints on the density of the martian crust. *Journal of Geophysical Research: Planets*, *119*, 1707–1727. https://doi.org/10.1002/2014JE004642

Brasser, R. (2013). The formation of Mars: Building blocks and accretion time scale. *Space Science Reviews*, *174*(1), 11–25. https://doi.org/10.1007/s11214-012-9904-2

Breuer, D., & Moore, W. B. (2015). Dynamics and thermal history of the terrestrial planets, the moon, and Io. *Treatise on Geophysics*, *10*(Second Ed.), 299–348. https://doi.org/10.1016/B978-0-444-53802-4.00173-1

Breuer, D., Plesa, A.-C., Tosi, N., & Grott, M. (2016). Water in the martian interior—The geodynamical perspective. *Meteoritic and Planetary Science*, *51*(11), 1959–1992. https://doi.org/10.1111/maps.12727

Breuer, D., & Spohn, T. (2006). Viscosity of the martian mantle and its initial temperature: Constraints from crustal formation history and the evolution of the magnetic field. *Planetary and Space Science*, *54*, 153–169. https://doi.org/10.1016/j.pss.2005.08.008

Burov, E.-B., & Diament, M. (1995). The effective elastic thickness (Te) of continental lithosphere: What does it really mean? *Journal of Geophysical Research*, *100*, 3905–3927.

19448007, 2018, 22, Downloaded from https://agupubs.onlinelibrary.wiley.com/doi/10.1029/2018GL080728 by Cochrane Colombia, Wiley Online Library on [24/06/2025]. See the Terms and Conditions (https://onlinelibrary.wiley.com/terms-and-conditions) on Wiley Online Library for rules of use; OA articles are governed by the applicable Creative Commons License

Cheung, K. K., & King, S. D. (2014). Geophysical evidence supports migration of Tharsis volcanism on Mars. *Journal of Geophysical Research: Planets*, *119*, 1078–1085. https://doi.org/10.1002/2014JE004632

Citron, R. I., Manga, M., & Tan, E. (2018). A hybrid origin of the martian crustal dichotomy: Degree-1 convection antipodal to a giant impact. *Earth and Planetary Science Letters*, *491*, 58–66. https://doi.org/10.1016/j.epsl.2018.03.031

Dixon, N. A., & Durham, W. B. (2018). Measurement of activation volume for creep of dry olivine at upper-mantle conditions. *Journal of Geophysical Research: Solid Earth*, *123*. https://doi.org/10.1029/2018JB015853

Dreibus, G., & Wänke, H. (1985). Mars, a volatile-rich planet. *Meteoritics*, *20*, 367–382.

Elkins-Tanton, L. T., Zaranek, S. E., Parmentier, E. M., & Hess, P. C. (2005). Early magnetic field and magmatic activity on Mars from magma ocean cumulate overturn. *Earth and Planetary Science Letters*, *236*, 1–12.

Filiberto, J. (2017). Geochemistry of martian basalts with constraints on magma genesis. *Chemical Geology*, *466*, 1–14.

Filiberto, J., Baratoux, D., Beaty, D., Breuer, D., Farcy, B. J., Grott, M., et al. (2016). A review of volatiles in the martian interior. *Meteoritics & Planetary Science*, *51*(11), 1935–1958.

Filiberto, J., & Dasgupta, R. (2015). Constraints on the depth and thermal vigor of melting in the martian mantle. *Journal of Geophysical Research: Planets*, *120*, 109–122. https://doi.org/10.1002/2014JE004745

Filiberto, J., Gross, J., & McCubbin, F. M. (2016). Constraints on the water, chlorine, and fluorine content of the martian mantle. *Meteoritics & Planetary Science*, *51*(11), 2023–2035.

Fraeman, A. A., & Korenaga, J. (2010). The influence of mantle melting on the evolution of Mars. *Icarus*, *210*(1), 43–57. https://doi.org/10.1016/j.icarus.2010.06.030

Genova, A., Goossens, S., Lemoine, F. G., Mazarico, E., Neumann, G. A., Smith, D. E., & Zuber, M. T. (2016). Seasonal and static gravity field of Mars from MGS, Mars Odyssey and MRO radio science. *Icarus*, *272*(Supplement C), 228–245. https://doi.org/10.1016/j.icarus.2016.02.050

Golabek, G., Keller, T., Gerya, T. V., Zhu, G., Tackley, P. J., & Connolly, J. A. D. (2011). Origin of the martian dichotomy and Tharsis from a giant impact causing massive magmatism. *Icarus*, *215*, 346–357. https://doi.org/10.1016/j.icarus.2011.06.012

Goossens, S., Sabaka, T. J., Genova, A., Mazarico, E., Nicholas, J. B., & Neumann, G. A. (2017). Evidence for a low bulk crustal density for Mars from gravity and topography. *Geophysical Research Letters*, *44*, 7686–7694. https://doi.org/10.1002/2017GL074172

Greeley, R., & Schneid, B. D. (1991). Magma generation on Mars: Amounts, rates, and comparisons with Earth, moon, and Venus. *Science*, *254*(5034), 996–998. https://doi.org/10.1126/science.254.5034.996

Grott, M., Baratoux, D., Hauber, E., Sautter, V., Mustard, J., Gasnault, O., et al. (2013). Long-term evolution of the martian crust-mantle system. *Space Science Review*, *172*(1), 49–111. https://doi.org/10.1007/s11214-012-9948-3

Grott, M., & Breuer, D. (2008). The evolution of the martian elastic lithosphere and implications for crustal and mantle rheology. *Icarus*, *193*, 503–515. https://doi.org/10.1016/j.icarus.2007.08.015

Grott, M., & Breuer, D. (2009). Implications of large elastic thicknesses for the composition and current thermal state of Mars. *Icarus*, *201*, 540–548. https://doi.org/10.1016/j.icarus.2009.01.020

Grott, M., & Breuer, D. (2010). On the spatial variability of the martian elastic lithosphere thickness: Evidence for mantle plumes? *Journal of Geophysical Research*, *115*, E03005. https://doi.org/10.1029/2009JE003456

Hahn, B. C., McLennan, S. M., & Klein, E. C. (2011). Martian surface heat production and crustal heat flow from Mars Odyssey gamma-ray spectrometry. *Geophysical Research Letters*, *38*, L14203. https://doi.org/10.1029/2011GL047435

Hauber, E., Brož, P., Jagert, F., Jodłowski, P., & Platz, T. (2011). Very recent and wide-spread basaltic volcanism on Mars. *Geophysical Research Letters*, *38*, L10201. https://doi.org/10.1029/2011GL047310

Hauck, S. A., & Phillips, R. P. (2002). Thermal and crustal evolution of Mars. *Journal of Geophysical Research*, *107*(E7), 5052. https://doi.org/10.1029/2001JE001801

Hirth, G., & Kohlstedt, D. (2003). *Rheology of the upper mantle and the mantle wedge: A view from the experimentalists* (pp. 83–105). Washington, DC: American Geophysical Union. https://doi.org/10.1029/138GM06

Hüttig, C., & Stemmer, K. (2008a). Finite volume discretization for dynamic viscosities on Voronoi grids. *Physics of the Earth and Planetary Interios*, *171*(1–4), 137–146. https://doi.org/10.1016/j.pepi.2008.07.007

Hüttig, C., & Stemmer, K. (2008b). The spiral grid: A new approach to discretize the sphere and its application to mantle convection. *Geochemistry, Geophysics, Geosystems*, *9*, Q02018. https://doi.org/10.1029/2007GC001581

Hüttig, C., Tosi, N., & Moore, W. B. (2013). An improved formulation of the incompressible Navier-Stokes equations with variable viscosity. *Physics of the Earth and Planetary Interios*, *40*, 113–129.

Hynek, B. M., Robbins, S. J., Šrámek, O., & Zhong, S. J. (2011). Geological evidence for a migrating Tharsis plume on early Mars. *Earth and Planetary Science Letters*, *310*(3–4), 327–333.

Jackson, I., Faul, U. H., Suetsugu, D., Bina, C., Inoue, T., & Jellinek, M. (2010). Grainsize-sensitive viscoelastic relaxation in olivine: Towards a robust laboratory-based model for seismological application. *Physics of the Earth and Planetary Interiors*, *183*, 151–163. https://doi.org/10.1016/j.pepi.2010.09.005

Karato, S. I., & Wu, P. (1993). Rheology of the upper mantle: A synthesis. *Science*, *260*, 771–778.

Keller, T., & Tackley, P. J. (2009). Towards self-consistent modeling of the martian dichotomy: The influence of one-ridge convection on crustal thickness distribution. *Icarus*, *202*, 429–443.

Khan, A., Liebske, C., Rozel, A., Rivoldini, A., Nimmo, F., Connolly, J. A. D., et al. (2017). A geophysical perspective on the bulk composition of Mars. *Journal of Geophysical Research: Planets*, *123*, 575–611. https://doi.org/10.1002/2017JE005371

Kiefer, W. S., Filiberto, J., Sandu, C., & Li, Q. (2015). The effects of mantle composition on the peridotite solidus: Implications for the magmatic history of Mars. *Geochimica et Cosmochimica Acta*, *162*, 247–258.

Kiefer, W. S., & Li, Q. (2009). Mantle convection controls the observed lateral variations in lithospheric thickness on present-day Mars. *Geophysical Research Letters*, *36*, L18203. https://doi.org/10.1029/2009GL039827

Kiefer, W. S., & Li, Q. (2016). Water undersaturated mantle plume volcanism on present-day Mars. *Meteoritics & Planetary Science*, *51*(11), 1993–2010.

Konopliv, A. S., Asmar, S. W., Folkner, W. M., Karatekin, Ö., Nunes, D. C., Smrekar, S. E., et al. (2011). Mars high resolution gravity fields from MRO, Mars seasonal gravity, and other dynamical parameters. *Icarus*, *211*, 401–428. https://doi.org/10.1016/j.icarus.2010.10.004

Konopliv, A. S., Park, R. S., & Folkner, W. M. (2016). An improved JPL Mars gravity field and orientation from Mars orbiter and lander tracking data. *Icarus*, *274*(Supplement C), 253–260. https://doi.org/10.1016/j.icarus.2016.02.052

Lainey, V. (2016). Quantification of tidal parameters from Solar System data. *Celestial Mechanics and Dynamical Astronomy*, *126*, 145–156. https://doi.org/10.1007/s10569-016-9695-y

Maurice, M., Tosi, N., Samuel, H., Plesa, A.-C., Hüttig, C., & Breuer, D. (2017). Onset of solid-state mantle convection and mixing during magma ocean solidification. *Journal of Geophysical Research: Planets*, *122*, 577–598. https://doi.org/10.1002/2016JE005250

19448007, 2018, 22, Downloaded from https://agupubs.onlinelibrary.wiley.com/doi/10.1029/2018GL080728 by Cochrane Colombia, Wiley Online Library on [24/06/2025]. See the Terms and Conditions (https://onlinelibrary.wiley.com/terms-and-conditions) on Wiley Online Library for rules of use; OA articles are governed by the applicable Creative Commons License

McCubbin, F. M., Boyce, J. W., Srinivasan, P., Santos, A. R., Elardo, S. M., Filiberto, J., et al. (2016). Heterogeneous distribution of H_2O in the martian interior: Implications for the abundance of H_2O in depleted and enriched mantle sources. *Meteoritics & Planetary Science*, *51*(11), 2036–2060.

McNutt, M. K. (1984). Lithospheric flexure and thermal anomalies. *Journal of Geophysical Research*, *89*(B13), 11,180–11,194. https://doi.org/10.1029/JB089iB13p11180

Moore, W. B., & Schubert, G. (2000). Note: The tidal response of Europa. *Icarus*, *147*, 317–319. https://doi.org/10.1006/icar.2000.6460

Morschhauser, A., Grott, M., & Breuer, D. (2011). Crustal recycling, mantle dehydration, and the thermal evolution of Mars. *Icarus*, *212*, 541–558. https://doi.org/10.1016/j.icarus.2010.12.028

Musselwhite, D. S., Dalton, H. A., Kiefer, W. S., & Treiman, A. H. (2006). Experimental petrology of the basaltic shergottite Yamato-980459: Implications for the thermal structure of the martian mantle. *Meteoritics & Planetary Science*, *41*(9), 1271–1290.

Neukum, G., Jaumann, R., Hoffmann, H., Hauber, E., Head, J., Basilevsky, A., et al. (2004). Recent and episodic volcanic and glacial activity on Mars revealed by the high resolution stereo camera. *Nature*, *432*, 971–979.

Newsom, H. E., Crumpler, L. S., Reedy, R. C., Petersen, M. T., Newsom, G. C., Evans, L. G., et al. (2007). Geochemistry of martian soil and bedrock in mantled and less mantled terrains with gamma ray data from Mars Odyssey. *Journal of Geophysical Research*, *112*, E03S12. https://doi.org/10.1029/2006JE002680

Nimmo, F., & Faul, U. H. (2013). Dissipation at tidal and seismic frequencies in a melt-free, anhydrous Mars. *Journal of Geophysical Research: Planets*, *118*, 2558–2569. https://doi.org/10.1002/2013JE004499

Nimmo, F., & Tanaka, K. (2005). Early crustal evolution of Mars. *Annual Review of Earth and Planetary Sciences*, *33*(1), 133–161. https://doi.org/10.1146/annurev.earth.33.092203.122637

Padovan, S., Margot, J.-L., Hauck, S. A., Moore, W. B., & Solomon, S. C. (2014). The tides of Mercury and possible implications for its interior structure. *Journal of Geophysical Research: Planets*, *119*, 850–866. https://doi.org/10.1002/2013JE004459

Phillips, R. J., Zuber, M. T., Smrekar, S. E., Mellon, M. T., Head, J. W., Tanaka, K. L., et al. (2008). Mars north polar deposits: Stratigraphy, age, and geodynamical response. *Science*, *320*(5880), 1182–1185. https://doi.org/10.1126/science.1157546

Plesa, A.-C., & Breuer, D. (2014). Partial melting in one-plate planets: Implications for thermo-chemical and atmospheric evolution. *Planetary and Space Science*, *98*, 50–65. https://doi.org/10.1016/j.pss.2013.10.007, planetary evolution and life.

Plesa, A.-C., Grott, M., Tosi, N., Breuer, D., Spohn, T., & Wieczorek, M. A. (2016). How large are present-day heat flux variations across the surface of Mars? *Journal of Geophysical Research: Planets*, *121*, 2386–2403. https://doi.org/10.1002/2016JE005126

Plesa, A.-C., Tosi, N., & Breuer, D. (2014). Can a fractionally crystallized magma ocean explain the thermo-chemical evolution of Mars? *Earth and Planetary Science Letters*, *403*, 225–235. https://doi.org/10.1016/j.epsl.2014.06.034

Plesa, A. C., Tosi, N., Grott, M., & Breuer, D. (2015). Thermal evolution and Urey ratio of Mars. *Journal of Geophysical Research: Planets*, *120*, 995–1010. https://doi.org/10.1002/2014JE004748

Raterron, P., Holyoke, C., Tokle, L., Hilairet, N., Merkel, S., Hirth, G., & Weidner, D. (2017). Effect of iron content on olivine viscosity and implications for the Martian mantle, 48th. LPSC, The Woodlands, Texas, Abstract 1553.

Rivoldini, A., Hoolst, T. V., Verhoeven, O., Mocquet, A., & Dehant, V. (2011). Geodesy constraints on the interior structure and composition of Mars. *Icarus*, *213*(2), 451–472. https://doi.org/10.1016/j.icarus.2011.03.024

Roberts, J., & Arkani-Hamed, J. (2017). Effects of basin-forming impacts on the thermal evolution and magnetic field of Mars. *Earth and Planetary Science Letters*, *478*, 192–202. https://doi.org/10.1016/j.epsl.2017.08.031

Roberts, J. H., & Zhong, S. (2006). Degree-1 convection in the martian mantle and the origin of the hemispheric dichotomy. *Journal of Geophysical Research*, *111*, E06013. https://doi.org/10.1029/2005JE002668

Ruedas, T., & Breuer, D. (2017). On the relative importance of thermal and chemical buoyancy in regular and impact-induced melting in a Mars-like planet. *Journal of Geophysical Research: Planets*, *122*, 1554–1579. https://doi.org/10.1002/2016JE005221

Ruedas, T., Tackley, P. J., & Solomon, S. C. (2013). Thermal and compositional evolution of the martian mantle: Effects of phase transitions and melting. *Physics of the Earth and Planetary Interios*, *216*, 32–58. https://doi.org/10.1016/j.pepi.2012.12.002

Sautter, V., Toplis, M. J., Beck, P., Mangold, N., Wiens, R., Pinet, P., et al. (2016). Magmatic complexity on early Mars as seen through a combination of orbital, in-situ and meteorite data. *Lithos*, *254–255*, 36–52. https://doi.org/10.1016/j.lithos.2016.02.023

Schubert, G., & Spohn, T. (1990). Thermal history of Mars and the sulfur content of its core. *Journal of Geophysical Research*, *95*(B9), 14,095–14,104. https://doi.org/10.1029/JB095iB09p14095

Schumacher, S., & Breuer, D. (2006). Influence of a variable thermal conductivity on the thermochemical evolution of Mars. *Journal of Geophysical Research*, *111*, E02006. https://doi.org/10.1029/2007GL030083

Taylor, G. J., Boynton, W., Brückner, J., Wänke, H., Dreibus, G., Kerry, K., et al. (2006). Bulk composition and early differentiation of Mars. *Journal of Geophysical Research*, *111*, E03S10. https://doi.org/10.1029/2005JE002645

Thiriet, M., Michaut, C., Breuer, D., & Plesa, A.-C. (2018). Hemispheric dichotomy in lithosphere thickness on Mars caused by differences in crustal structure and composition. *Journal of Geophysical Research: Planets*, *123*, 823–848. https://doi.org/10.1002/2017JE005431

Tosi, N., Plesa, A.-C., & Breuer, D. (2013). Overturn and evolution of a crystallized magma ocean: A numerical parameter study for Mars. *Journal of Geophysical Research: Planets*, *118*, 1512–1528. https://doi.org/10.1002/jgre.20109

Tosi, N., Yuen, D. A., de Koker, N., & Wentzcovitch, R. M. (2013). Mantle dynamics with pressure- and temperature-dependent thermal expansivity and conductivity. *Physics of the Earth and Planetary Interios*, *217*, 48–58. https://doi.org/10.1016/j.pepi.2013.02.004

Van Hoolst, T., Dehant, V., Roosbeek, F., & Lognonné, P. (2003). Tidally induced surface displacements, external potential variations, and gravity variations on mars. *Icarus*, *161*(2), 281–296. https://doi.org/10.1016/S0019-1035(02)00045-3

Wänke, H., & Dreibus, G. (1994). Chemistry and accretion of Mars. *Philosophical Transactions of the Royal Society London*, *A349*, 2134–2137.

Werner, S. C. (2009). The global martian volcanic evolutionary history. *Icarus*, *201*, 44–68. https://doi.org/10.1016/j.icarus.2008.12.019

Wieczorek, M. A. (2008). Constraints on the composition of the martian south polar cap from gravity and topography. *Icarus*, *196*(2), 506–517. https://doi.org/10.1016/j.icarus.2007.10.026

Wieczorek, M. A., Neumann, G. A., Nimmo, F., Kiefer, W. S., Taylor, G. J., Melosh, H. J., et al. (2013). The crust of the moon as seen by GRAIL. *Science*, *339*(6120), 671–675. https://doi.org/10.1126/science.1231530

Wieczorek, M. A., & Zuber, M. T. (2004). Thickness of the martian crust: Improved constraints from geoid-to-topography ratios. *Journal of Geophysical Research*, *109*, E01009. https://doi.org/10.1029/2003JE002153

Yoder, C. F., Konopliv, A. S., Yuan, D. N., Standish, E. M., & Folkner, W. M. (2003). Fluid core size of Mars from detection of the solar tide. *Science*, *300*, 299–303. https://doi.org/10.1126/science.1079645

Zhao, Y.-H., Zimmerman, M. E., & Kohlstedt, D. L. (2009). Effect of iron content on the creep behavior of olivine: 1. Anhydrous conditions. *Earth and Planetary Science Letters*, *287*, 229–240. https://doi.org/10.1016/j.epsl.2009.08.006

19448007, 2018, 22, Downloaded from https://agupubs.onlinelibrary.wiley.com/doi/10.1029/2018GL080728 by Cochrane Colombia, Wiley Online Library on [24/06/2025]. See the Terms and Conditions (https://onlinelibrary.wiley.com/terms-and-conditions) on Wiley Online Library for rules of use; OA articles are governed by the applicable Creative Commons License

Zhong, S. (2009). Migration of Tharsis volcanism on Mars caused by differential rotation of the lithosphere. *Nature Geoscience*, *2*, 19–23. https://doi.org/10.1038/NGEO392

Zhong, S., & Roberts, J. H. (2003). On the support of the Tharsis Rise on Mars. *Earth and Planetary Science Letters*, *214*(1), 1–9.

Šrámek, O., & Zhong, S. (2012). Martian crustal dichotomy and Tharsis formation by partial melting coupled to early plume migration. *Journal of Geophysical Research*, *117*, E01005. https://doi.org/10.1029/2011JE003867

19448007, 2018, 22, Downloaded from https://agupubs.onlinelibrary.wiley.com/doi/10.1029/2018GL080728 by Cochrane Colombia, Wiley Online Library on [24/06/2025]. See the Terms and Conditions (https://onlinelibrary.wiley.com/terms-and-conditions) on Wiley Online Library for rules of use; OA articles are governed by the applicable Creative Commons License